Journal of Applied Physics ARTICLE scitation.org/journal/jap

Design and optimization of a magnet for magnetocaloric refrigeration

Cite as: J. Appl. Phys. **126**, 164502 (2019); doi: 10.1063/1.5114702
Submitted: 11 June 2019 · Accepted: 4 October 2019 ·
Published Online: 22 October 2019

Jesús Francisco Beltrán-López, Elías Palacios,[a] David Velázquez, and Ramón Burriel

AFFILIATIONS

Instituto de Ciencia de Materiales de Aragón and Departamento de Física de la Materia Condensada, CSIC—University of Zaragoza, Pedro Cerbuna 12, 50009 Zaragoza, Spain

[a]**Electronic mail:** elias@unizar.es

ABSTRACT

The magnetic field source is the most expensive element of a magnetic refrigeration device. The design of an efficient magnet with high and low field regions, using reduced volumes of permanent magnets, is of paramount importance for the practical application of this new technology. A two-pole rotary magnet formed by sectors of oriented hard magnets and soft iron pieces is optimized in angular width and magnetization direction of each sector. A quadratic approximation is used for the optimization of the defining angles. This procedure provides the parameters that result in extreme values of a given functional F, defined as an efficiency variable of the working device. The procedure also gives the correlation between parameters and the relative importance of the deviations with respect to their mathematical optimal values. An optimized magnet has also been built, and the resulting calculated fields are compared with experimental measurements in the real system.

I. INTRODUCTION

After the discovery of the so-called "giant magnetocaloric effect"[1] (GMCE), magnetic refrigeration at room temperature (RT) became a competitive technology to other conventional methods. To date, more than 50 prototypes of refrigeration systems have been published or patented. The most important and expensive component of such a system is the magnetic field source that, for a home device, is usually based on permanent magnets of NdFeB alloys.[2] In this context, the efficiency of a magnet has been quantified by Björk *et al.*[3] with an expression that applied to our magnet would be

$$\Lambda_{cool} = \left(\langle B_{high}^{2/3}\rangle - \langle B_{low}^{2/3}\rangle\right)\frac{V_{field}}{V_{mag}}P_{field}, \quad (1)$$

where $\langle B_{high}^{2/3}\rangle$ is the average of $B_{high}^{2/3}$ in the high field region (similarly, $\langle B_{low}^{2/3}\rangle$ in the low flux density region), with B being the flux density in tesla. V_{field} is the volume of the high field region, V_{mag} is the volume of the permanent magnets, and P_{field} is the time fraction in which the active magnetic regenerator (AMR) is in the high flux region. The power 2/3 arises from the dependence of the magnetocaloric effect (MCE) near the Curie temperature in typical materials having a second-order magnetic transition. In this expression, it turns out that, for a given design, a near zero field in the low field region is more important than reaching a very high field in the high field region. This parameter Λ_{cool} has been increasing since the early 2000s from $\Lambda_{cool} = 0.05$[4] to $\Lambda_{cool} = 0.21$ with a four-pole magnet.[5] A further derivation of this design by Eriksen *et al.*[6] replaces almost one half of the permanent magnet material with soft iron, with only a small reduction of the maximum field but achieving a high increase of Λ_{cool}. However, this design has small regions with demagnetization risk of the magnets, i.e., regions of the permanent magnets where **B** is small or even opposite to the magnetization **M**. These regions should be made of a harder magnetic material, which usually implies a lower magnetization. This smart design can be improved by optimizing the angular thickness and magnetization directions of the NdFeB sectors. Our work deals with the optimization of these parameters and, for this purpose, a functional $F(x_i)$ of the optimizable parameters x_i is defined with a view to its application in magnetic refrigeration.

II. DESIGN AND OPTIMIZATION

The design starts with the two-pole magnet reported by Eriksen *et al.*[6] The variable parameters are shown in Fig. 1.

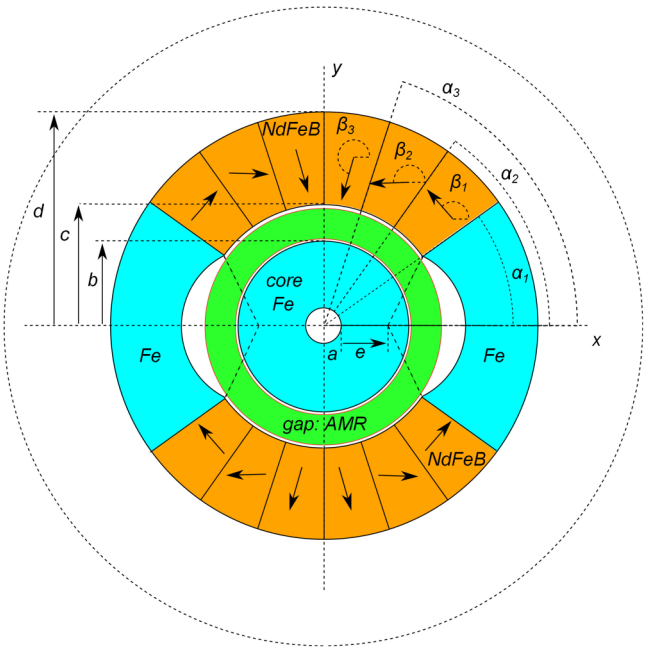

FIG. 1. Cross section of the magnet's initial design, following the model of Eriksen *et al.*,[6] with the definition of the variable parameters. The outer dashed circle marks the limit for the finite element method (FEM) calculation ($1.5 \cdot d = 150$ mm), where the radial component of **B** has been fixed to zero.

In order to save computing time, the calculation has been made in 2D, considering that this simplification has no relevant effect on the optimized parameters, for the chosen dimensions. These are the radii a, b, c, d, the azimuthal angles of the iron-magnet and magnet-magnet interphases, α_1, α_2, α_3, and the angles defining the direction of magnetization of each sector, $\beta_1, \beta_2, \beta_3$. The central blue zone (core) is made of a magnetically soft iron with negligible anisotropy and hysteresis. The lateral iron sectors are under a nearly static magnetic field. Finally, the empty meniscus between the AMR and each iron sector has circular boundaries, one of them with the center at $x = a + e$, $y = 0$, with e being another adjustable parameter. In Fig. 1, the fields **B**, **H**, and **M** are symmetric with respect to the y-axis and antisymmetric with respect to the x-axis.

For our purpose, the green region in Fig. 1 (gap) is filled with a magnetocaloric material divided into eight sectors, covering an angular range of 45° each. Every sector acts as an active magnetic regenerator (AMR) along the axial direction, z-axis, perpendicular to Fig. 1. In the normal working procedure, a cold fluid flows through the AMRs in the two low field regions toward a cold thermal source, while a warm one flows through the sectors in the two high field regions toward a hot sink. The fluid is at rest in the four regions of the intermediate field. The outer part of the magnet assembly (rotor), including permanent magnets and iron sectors, turns around the z axis and the fluid motion is accordingly synchronized in each sector, when the magnetic flux is high, low, or intermediate.

To determine the magnetic field at every point, the magnetic behavior of the materials has been modeled as follows. Far enough from reaching the coercive field, the permanent magnets of NdFeB alloys behave very accurately as media with constant magnetization **M**. The core and two iron sectors are made of soft iron and low-carbon steel, respectively. They can be chosen among a wide variety of materials. For the calculations, iron is assumed to give a linear dependence $\mathbf{B} = \mu(\mathrm{Fe})\mathbf{H}$ with relative permeability $\mu_r(\mathrm{Fe}) = \mu/\mu_0 = 200$; nevertheless, this parameter has a small effect on the field, provided that $\mu_r(\mathrm{Fe}) \gg 1$. The actual values of $\mu_r(\mathrm{Fe})$ exceed safely 200, adding a negligible reluctance to the magnetic circuit. The value assumed in the calculations assures an upper limit for the flux leakage to the gap in the region of lowest flux density. The magnetization of the AMR depends on temperature and field in a nontrivial way. In reality, the magnetic work received by an AMR per cycle and unit volume, $W_m = \oint \mathbf{M} \cdot d\mathbf{B}$ comes explicitly from the dependence of μ on temperature. The not always linear, nor simple, $B(H)$ dependence of the AMR has some measurable effect on the field,[7] but it is not decisive. For the sake of simplicity, a linear dependence has been assumed with constant $\mu = 2\mu_0$, a typical average value for a magnetocaloric material near its Curie temperature. Finally, the permeability of air is taken as μ_0. Under these conditions, **M** is assumed to be a constant vector in the permanent magnets, $\nabla \cdot \mathbf{H} = \nabla \cdot \mathbf{B}/\mu_0 - \nabla \cdot \mathbf{M} = 0$. In linear homogeneous media $\mathbf{B} = \mu\mathbf{H} \Rightarrow \nabla \cdot \mathbf{H} = \nabla(1/\mu) \cdot \mathbf{B} + \nabla \cdot \mathbf{B}/\mu = 0$. In both cases, the magnetic field, $\mathbf{H} = -\nabla\phi$, derives from a scalar potential ϕ obeying the Laplace equation in every region, with the boundary conditions of continuity of the normal components of **B** and the parallel components of **H** at every interphase. The scalar potential has been determined by the finite element method (FEM) with triangular meshing, using the software GMESH[8] and GETDP[9] for solving the system of equations.

In a further simplification, all permanent magnets are assumed to have the same constant M, changing only the direction from one sector to another. Therefore, M is a scale factor. The flux density data are given as the dimensionless quantity $B/\mu_0 M$. For an initial calculation using the FEM, a meshing of 8473 nodes and 16 752 triangles has been made. These numbers change slightly with every modification in the system's parameters. The size has been chosen by making the calculations with smaller and smaller triangles until the difference in the results was negligible. B is found to be intense near the corners of the regions. Theoretically $B \to \infty$ with the logarithm of the distance to any corner, but the assumption of constant **M** is not realistic near a corner and the real corners are not mathematical vertices. Leaving the space of the regenerators empty (making $\mu_{AMR} = \mu_0$), the average $B(\theta)$ over the radius of the gap region agrees with the calculation of Eriksen *et al.*[6] using the same geometry and NdFeB material described in this reference. Considering $\mu_{AMR} = 2\mu_0$, the maximum field in the gap increases markedly. B is very small, meaning $\mathbf{H} \simeq -\mathbf{M}$, near the top and bottom of the magnet, as also seen in Fig. 2, being the only regions with demagnetization risk. Moreover, the high field resulting near the central hole of Fig. 1 could have a risk of saturation of the iron core, which can be reduced by decreasing the parameter a. In Fig. 2, the space occupied by one of the eight AMRs, when its center makes a polar angle θ with the maximum field position, is marked by a solid black line. Each AMR covers an angle $2\alpha = 45°$.

Instead of the usual maximum gradient method, for the optimization we use the quasi-Newton method to find the zero of the

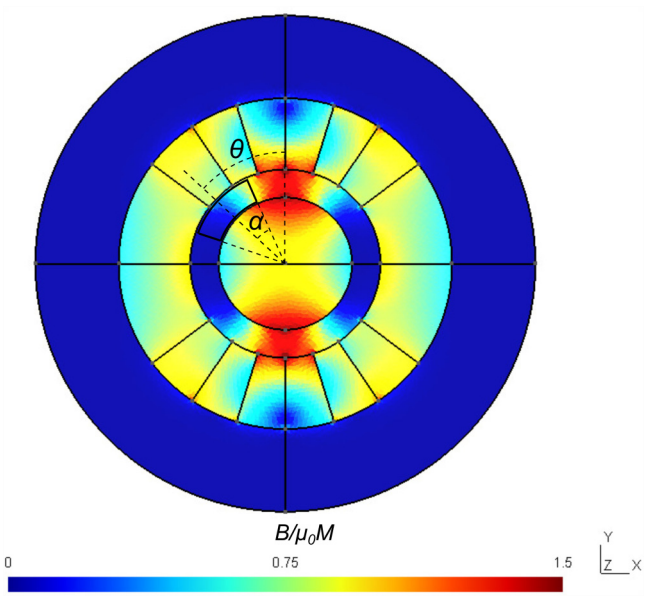

FIG. 2. $B/\mu_0 M$ for a typical FEM calculation. The sector limited by a solid black line represents one of the eight AMRs, in a position determined by the polar angle θ between the center of this AMR and that of maximum field. Each AMR covers an angle $2\alpha = 45°$.

gradient of a functional, given by a quadratic approximation.[10] The optimized functional $F(x_i)$, of N adjustable parameters x_i $(i = 1, 2, \ldots, N)$, will be defined below, according to the specifications of the physical system. $F(x_i)$ is minimized or maximized for the values of x_i. This procedure not only gives the optimal parameters but also the relative importance of each one and whether a given parameter is optimizable or not. Near a critical point (maximum, minimum, or saddle point), $F(x_i)$ can be expanded in a Taylor series of several variables up to second order as

$$\begin{aligned} F(x_i) &= F(x_{i0}) + \sum_{i=1}^{N} \left(\frac{\partial F}{\partial x_i}\right)_{x_{i0}} (x_i - x_{i0}) \\ &\quad + \frac{1}{2}\sum_{i=1}^{N}\sum_{j=1}^{N} \left(\frac{\partial^2 F}{\partial x_i \partial x_j}\right)_{x_{i0}} (x_i - x_{i0})(x_j - x_{j0}) + \cdots \\ &= F(x_{i0}) + \sum_{i=1}^{N} B_i (x_i - x_{i0}) + \frac{1}{2}\sum_{i=1}^{N}\sum_{j=1}^{N} A_{ij}(x_i - x_{i0})(x_j - x_{j0}) + \cdots \end{aligned} \tag{2}$$

with vector (x_{i0}) being an arbitrary point in the parameter space. If we have some method to evaluate $F(x_i)$ for any set of parameters, the first and second derivatives can be evaluated taking small increments Δx_i by finite-difference approximations, with errors proportional to Δx_i^3. Defining, for each pair of increments $\Delta x_i = x_i - x_{i0}$ and $\Delta x_j = x_j - x_{j0}$,

$$\begin{aligned} F_0 &= F(x_{10}, \ldots, x_{i0}, \ldots, x_{j0}, \ldots, x_{N0}), \\ F_1 &= F(x_{10}, \ldots, x_{i0} - \Delta x_i, \ldots, x_{j0}, \ldots, x_{N0}), \\ F_2 &= F(x_{10}, \ldots, x_{i0} + \Delta x_i, \ldots, x_{j0}, \ldots, x_{N0}), \\ F_3 &= F(x_{10}, \ldots, x_{i0} - \Delta x_i, \ldots, x_{j0} - \Delta x_j, \ldots, x_{N0}), \\ F_4 &= F(x_{10}, \ldots, x_{i0} + \Delta x_i, \ldots, x_{j0} - \Delta x_j, \ldots, x_{N0}), \\ F_5 &= F(x_{10}, \ldots, x_{i0} - \Delta x_i, \ldots, x_{j0} + \Delta x_j, \ldots, x_{N0}), \\ F_6 &\equiv F(x_{10}, \ldots, x_{i0} + \Delta x_i, \ldots, x_{j0} + \Delta x_j, \ldots, x_{N0}), \end{aligned}$$

we have, up to second order in the increments,

$$\left(\frac{\partial F}{\partial x_i}\right)_{x_{i0}} = B_i \cong \frac{F_2 - F_1}{2\Delta x_i}, \tag{3}$$

$$\left(\frac{\partial^2 F}{\partial x_i^2}\right)_{x_{i0}} = A_{ii} \cong \frac{F_2 + F_1 - 2F_0}{\Delta x_i^2}, \tag{4}$$

$$\left(\frac{\partial^2 F}{\partial x_i \partial x_j}\right)_{x_{i0}} = A_{ij} \cong \frac{F_6 - F_5 - F_4 + F_3}{4\Delta x_i \Delta x_j}. \tag{5}$$

The quadratic expression, replacing the derivatives with the finite differences, is not merely an approximation of the Taylor series, but an interpolation formula that matches the exact functional $F(x_i)$ at (x_{i0}) and at points obtained from it by the increment of a single variable to $x_{i0} \pm \Delta x_i$, i.e., it matches exactly the F_0, F_1, F_2 values for each variable. The value of $F_6 - F_5 - F_4 + F_3$ for every pair of increments Δx_i, Δx_j is also exactly represented. A critical point $(x_{i,cr})$ is defined as obeying $\left(\frac{\partial F}{\partial x_i}\right)_{x_{i,cr}} = 0$, $\forall i = 1, \ldots, N$. Using the quadratic approximation leads to the linear system of equations,

$$\sum_{j=1}^{N} A_{ij}(x_{j,cr} - x_{j0}) + B_i = 0, \qquad i = 1, \ldots, N. \tag{6}$$

The solution $(x_{j,cr}, j = 1, \ldots, N)$ will surely correspond to a minimum if the matrix A is positive definite, to a maximum if negative definite, and to a saddle point if it has some positive and some negative eigenvalues. If an eigenvalue is zero, the corresponding eigenvector is a linear combination of increments which makes $F(x_i)$ locally invariant near $(x_{i,cr})$, up to third order in the increments. Like in a least squares optimization, which is a particular case of functional F, the approximation would be more accurate if (x_{i0}) is near the critical point, but the obtained solution $(x_{i,cr})$ can be taken as a new (x_{i0}) for iteration, until the convergence is reached within some allowed error.

The procedure, in principle, can be used to optimize the working parameters of a real system or a simulation, when F is an experimental result or comes from a complete computer simulation of a system. In such cases, as happens when a 3D FEM calculation becomes necessary, reducing the number of evaluations of F is vital. In each iteration, this procedure needs $2N + 1$ evaluations of $F(x_i)$ to obtain the first-order and direct second-order derivatives and $2N(N - 1)$ evaluations for the mixed second-order derivatives, or $2N^2 + 1$ evaluations in total. Each evaluation involves meshing, finite elements solution for the field, and numerical evaluation of $F(x_i)$ from the results. Note that a quadratic function of N variables has only $(N + 1)(N + 2)/2$ coefficients to be determined; this is, hence, the minimum number of evaluations of F to determine the

critical point, i.e., the critical point of the unique hyperparaboloid passing exactly through $(N+1)(N+2)/2$ given points. We therefore use an approximation involving more evaluations but giving the derivatives with a higher order of approximation. For small deviations with respect to (x_{i0}) and for the present approximation, the error in $F(x_i)$ is a combination of cubic terms in $x_i - x_{i0}$, $x_j - x_{j0}$, $x_k - x_{k0}$ $(i, j, k = 1, \ldots, N)$. The error in the first and second derivatives is quadratic since, for the first derivatives, the even terms of the Taylor expansion cancel in $F_2 - F_1$. The error in $F_2 - F_1$ is then cubic, and in $(F_2 - F_1)/\Delta x_i$ it is quadratic. Similarly, for the second derivatives, the cubic terms cancel in the expansion of $F_1 + F_2 - 2F_0$ and also in $F_6 - F_5 - F_4 + F_3$. The ratio of the number of evaluations used with respect to the minimum is $f = 2(2N^2+1)/[(N+1)(N+2)]$, with $1 \le f < 4$. For our case $N = 6$, $f = 2.61$. Finally, extending the Taylor series to higher order terms has no practical interest with many variables because the number of partial derivatives to be determined increases quickly. We will not discuss the general conditions for convergence of this procedure, but merely mention that it leads to a maximum of $F(x_i)$, in the present problem of optimizing a magnet, if the initial point is close enough to the maximum, that is, if the B_i vector is small, and especially if the hyperellipsoid centered at (x_{i0}) and with half-axes (Δx_i) contains the critical point. A detailed discussion of the convergence of the quasi-Newton method is given in Ref. 11.

Once the critical point $(x_{j,cr})$ has been found, the functional F can be expressed in terms of the increments with respect to $(x_{j,cr})$. This is, defining $x_i' = x_i - x_{i,cr}$, we have

$$F - F_0 \simeq \frac{1}{2}\sum_{i,j=1}^{N} A_{ij} x_i' x_j', \tag{7}$$

where the linear terms have vanished, since the first derivatives are zero at a critical point. As any symmetric matrix, A can be diagonalized by an orthogonal matrix O, made with the eigenvectors of A written in columns, in such a way that the diagonal elements of $A_d = O^t A O$ are the eigenvalues, λ_i. Using the new coordinates $y_i = \sum_j^N O_{ij}^t x_j'$ near the critical point, the quadratic approximation results in

$$F - F_0 \simeq \frac{1}{2}\sum_{i=1}^{N} \lambda_i y_i^2. \tag{8}$$

Therefore, the eigenvectors of A (columns of O) indicate the independent combinations of increments x_i', in such a way that the change of F with respect to the critical value produced by one single increment y_i is independent of any other y_j. The eigenvalues indicate how large an increment of F is produced by a given y_i. If every $\lambda_i > 0$, F is a minimum at $(x_{i,cr})$, if every $\lambda_i < 0$, F is a maximum, and if $\lambda_i > 0$ and $\lambda_j < 0$ for some i and j, it is a saddle point. If one $\lambda_i = 0$, F is locally invariant, indicating that F does not vary for small changes of this particular parameter y_i, up to second order in y_i.

Now, we will discuss about the functional to be optimized. The magnet is intended for a magnetic refrigerator. The eight independent AMRs are placed in the green region of Fig. 1, covering an angle of 45° each. The outer part of the magnet assembly rotates counterclockwise around the z axis, perpendicular to Fig. 1. To analyze the case, let us suppose that the AMRs rotate clockwise with constant angular speed and the outer part of the magnetic circuit is fixed. The liquid starts flowing when the right end of the analyzed AMR sector reaches the maximum field point, that is, when $\theta = \alpha$ in Fig. 2, and stops flowing when the left end leaves the maximum field point $(\theta = -\alpha)$. It also flows when the AMR is in the minimum field region (dark blue region of the gap, near the x axis) between $\theta = \alpha\text{-}\pi/2$ and $\theta = -\alpha\text{-}\pi/2$, with cold liquid flowing to the cold source. The same thing happens in the AMRs at their opposite positions, at $180° + \theta$. For these four AMRs, there is a dead time without flow between the high and low field regions (while the AMR turns $90° - 2\alpha$), allowing the field to change from high to low values. During this dead time, the other four AMRs are active, with liquid flow, in the maximum or minimum field regions.

Regarding the application, the important quantity is the average field over one AMR. The field profile is symmetric with respect to the maximum and minimum, therefore, the average effective field, when the center of an AMR is near the position $\theta_0 = 0$ or 90°, is given by

$$\langle B \rangle = \frac{1}{\alpha(c^2 - b^2)} \int_b^c r dr \int_{\theta_0 - \alpha}^{\theta_0 + \alpha} B(r, \theta) d\theta. \tag{9}$$

Computing $\langle B \rangle$ for the highest and lowest field zones, the maximum MCE will be obtained for the largest difference. Consequently, the quantity to be maximized is $F = (\langle B_{high} \rangle - \langle B_{low} \rangle)/\mu_0 M$, computing $\langle B_{high} \rangle$ and $\langle B_{low} \rangle$ with Eq. (9) for the values $\theta_0 = 0°$ and 90°, respectively.

As pointed out in Ref. 3, the MCE can be proportional to the average of another power of B. Moreover, for the net cooling power, the field should be averaged over the volume of one AMR, and over the time the heat exchange liquid is flowing through it. The flow starts when the right side of the AMR reaches the maximum field position, $\theta = \alpha$ in Fig. 2, and stops when the left side reaches the maximum field point, $\theta = -\alpha$. Similarly, at the minimum field position. By symmetry, the average can be calculated as an integral between 0 and 2α (or between 90° and $90° + 2\alpha$), but considering that the maximum field $B(r, 0)$ is always acting on some point of the AMR, while $B(r, \theta)$ is acting only during a shorter time, tending to zero at the starting $(\theta = \alpha)$ and at the end $(\theta = -\alpha)$ of liquid flow. This effect could be taken into account in the functional to be optimized including a weighting factor. Equation (9) would change to

$$\langle B^n \rangle = \frac{1}{\alpha^2(c^2 - b^2)} \int_b^c r dr \int_{\theta_0}^{\theta_0 + 2\alpha} B^n(r, \theta)(2\alpha - \theta + \theta_0) d\theta. \tag{10}$$

Even the weighting factor could also consider the real flow of liquid, possibly not constant, when it is on. Nevertheless, as an example of the procedure we opted for simplicity, using Eq. (9).

Not all the parameters in Fig. 1 can be optimized. The fields **B**, **H** are invariant under the application of a scale factor to all lengths. The maximum flux density increases if the gap, $c - b$,

decreases (the maximum F occurs for $c - b = 0$, which is obviously useless), but it has to be determined by the desired volume of the AMRs. For a magnetic circuit made with permanent magnets having a constant M, taking a closed line along the circuit, Ampere's law states

$$\oint \mathbf{H} \cdot d\mathbf{l} = 0 \Rightarrow \int_{mag} \mathbf{M} \cdot d\mathbf{l} = \int_{mag} (B/\mu_0) dl + \int_{AMR} (B/\mu_{AMR}) dl + \int_{Fe} (B/\mu_{Fe}) dl \quad (11)$$

where the subscripts *mag*, *AMR*, and *Fe* refer to the parts of the circuit line of each material. The magnetic flux through the closed circuit, Φ, is constant. Taking the circuit with average cross sections for the different materials, A_{mag}, A_{AMR}, and A_{Fe}, one can write the total flux as a function of the average field in each region,

$$\Phi = \langle B_{mag} \rangle A_{mag} = \langle B_{AMR} \rangle A_{AMR} = \langle B_{Fe} \rangle A_{Fe}. \quad (12)$$

This allows to determine approximately the flux Φ and the average fields in each region by substituting B in Eq. (11) with its average value in each term, taken from Eq. (12). Thus, using $\Phi = \langle B_{AMR} \rangle A_{AMR}$ and the values taken for μ_{AMR} and μ_{Fe} results in

$$\langle B_{AMR} \rangle = \frac{\mu_0 \int_{mag} \mathbf{M} \cdot d\mathbf{l}}{A_{AMR} \left(\frac{l_{mag}}{A_{mag}} + \frac{l_{AMR}}{2A_{AMR}} + \frac{l_{Fe}}{200 A_{Fe}} \right)}, \quad (13)$$

where the parenthesis in the denominator is the reluctance of the magnetic circuit. For the dimensions of Fig. 1, the reluctance of the iron parts of the magnetic circuit happens to be negligible and $l_{AMR} \ll l_{mag}$, all cross sections being of similar magnitude. Then, for a quick and simple estimate, the flux is roughly determined by the magnetization M, the alignment of the vector $\mathbf{M}$ with the flux lines, and the length l_{mag} of the flux lines in the magnets. This means that $l_{AMR} = 2(c - b)$ can be increased up to values compatible with a small decrease of the magnetic flux (e.g., for $l_{AMR}/l_{mag} = 0.1$, a 5% decrease is expected with respect to the case $c - b = 0$).

The a parameter is also not optimizable, since the optimal value is zero. However, F is quite insensitive to a, since the core reluctance is negligible anyways. This parameter can be made high enough to save the material, but it should not be too high to prevent saturation of the iron core, since B reaches high values right next to the central hole, near the x axis.

III. NUMERICAL RESULTS

Let us consider for the initial parameters the approximate values deduced from the figures given by Eriksen *et al.*,[6] taking the lengths $a = 20$ mm, $b = 50$ mm, $c = 65$ mm, $d = 110$ mm, $e = 6$ mm, and angles $\alpha_1 = 33°$, $\alpha_2 = 52°$, $\alpha_3 = 71°$, $\beta_1 = 140°$, $\beta_2 = 195°$, and $\beta_3 = 250°$. With these parameters, the calculation of $B/\mu_0 M$ in an empty AMR of 45°, using the FEM, gives $F = \langle B_{high}/\mu_0 M \rangle - \langle B_{low}/\mu_0 M \rangle = 1.014$. The first derivatives B_i are high, and the quadratic approximation is not necessarily good. Moreover, we find that the field on the iron sectors can be near saturation. Calculations have been made with and without meniscus, and they show that, within the model, the meniscus has only a small effect on the total flux. On the one hand, it reduces the field in the gap near $\theta = 90°$, but it also reduces the cross section of the iron sector, increasing B where it can already be near saturation. Moreover, the material saving is not so important, since the iron sectors are not made of any critical material, and the absence of meniscus makes their construction easier.

We changed slightly these parameters to $a = 0$, $b = 40$ mm, $c = 57$ mm, $d = 100$ mm and canceled the meniscus, according to our specifications for the size of the magnet and the available volume for the magnetocaloric material. With these new parameters and keeping the same angles, we found $F = 0.974$ for a gap without any magnetocaloric material (the calculation for an empty gap is useful for a further comparison with measurements in the actual magnet) and $F = 1.162$ for a filled gap with a material having $\mu_r = 2$.

To optimize the magnet, we made an initial FEM calculation of F with single variations of the angles, one by one, taken the increments Δx_i and Δx_j in Eqs. (3) to (5) as 5°. We found a significant increase of the optimized functional value to $F = 1.236$ for $\mu_r = 2$ and the following parameters $x_1, \ldots, x_6$: $\alpha_1 = 35°$, $\alpha_2 = 55°$, $\alpha_3 = 75°$, $\beta_1 = 125°$, $\beta_2 = 170°$, and $\beta_3 = 235°$. These first optimized parameters have been taken as a starting point for the final optimization of our magnet. The complete optimization, following the procedure previously described, gave the final angles $\alpha_1 = 28.5°$, $\alpha_2 = 56.6°$, $\alpha_3 = 72.6°$, $\beta_1 = 128.9°$, $\beta_2 = 167.3°$, and $\beta_3 = 234.9°$, resulting in a value $F = 1.251$ for the functional.

Table I gives the initially optimized parameters x_{j0}, the vector of the first derivatives, (B_i), the symmetric Hessian matrix A and the values of F obtained from the initial parameters x_{j0} and from the final $x_{j,opt}$ values for the maximum F. It also reveals that the A matrix is negative definite, indicating that the critical point found is a maximum of F. The highest eigenvalue λ_1, in absolute value, corresponds mainly to β_3 variations combined with α_3. Both of them are by far the most influential parameters for the optimization of F, as can be seen from Eq. (8). On the other hand, the influence of α_1 deviations from the optimum value is one order of magnitude below. This detail will be considered for the construction of the actual system and can be understood in the framework of the magnetic circuit. When the iron and gap reluctances are negligible, an increment of α_1 produces a decrease of $l_{mag} \simeq 2(90 - \alpha_1)(\pi/180)(c + d)/2$, which results in approximately the same factor in the numerator and denominator of Eq. (13). F is then insensitive to α_1. Actually, $l_{mag} \simeq 4.3 l_{AMR}$ making such a simplification a bit crude. Also, small changes in β_1 and β_2 are almost irrelevant. The optimum F for the functional defined in this work is about 8% higher than the value obtained with the original parameters α_1 to β_3 of Ref. 6. A calculation of the optimized F has also been made for a system made with 16 sectors of permanent magnets (i.e., with parameters $\alpha_1, \ldots, \alpha_4, \beta_1, \ldots, \beta_4$), but the value of F only improves a mere 2%. Therefore, the actual design has been made with only 12 sectors of permanent magnets. Finally, the optimization of the e parameter, defining the center of the meniscus line, gave a very small difference of only 0.2% in F. As discussed above, the meniscus increases the reluctance of the gap for the direct flux

TABLE I. Matrix A and vector B as defined in Eq. (6), eigenvalues of A, λ_i (in decreasing absolute values), normalized eigenvectors, (v_i) (in columns), and solution of the system $A(x - x_0) = -B$ for the optimal increments. All matrix elements and eigenvalues in the table must be multiplied by 10^{-4}. Maximum and minimum average fields $\langle B_{high}\rangle$, $\langle B_{low}\rangle$ for $\theta_0 = 0$ and 90°, respectively, in units of $\mu_0 M$, defined in Eq. (9), and values of the functional $F = \langle B_{high}\rangle - \langle B_{low}\rangle$, for the initial, x_{j0}, and the optimized parameters, $x_{j,opt}$.

	α_1	α_2	α_3	β_1	β_2	β_3	
	35	55	75	125	170	235	
x_{j0}	A_{i1}	A_{i2}	A_{i3}	A_{i4}	A_{i5}	A_{i6}	B_i
A_{1j}	−4.072	−0.957	−0.073	0.685	0.704	−0.015	−25.80
A_{2j}	−0.957	−6.693	0.297	1.004	1.144	−0.044	4.269
A_{3j}	−0.073	0.297	−25.72	−0.118	3.129	0.6073	−52.28
A_{4j}	0.685	1.004	−0.118	−0.884	0.031	0.013	6.066
A_{5j}	0.704	1.144	3.129	0.031	−1.293	0.056	6.607
A_{6j}	−0.015	−0.044	0.6073	0.013	0.056	−34.86	9.164
λ_i	−37.94	−23.06	−7.48	−3.81	−0.90	−0.34	

	v_1	v_2	v_3	v_4	v_5	v_6
v_{1j}	−0.0012	0.0080	0.3289	0.9233	0.0177	0.1972
v_{2j}	0.0042	−0.0057	0.9079	−0.3665	−0.0105	0.2030
v_{3j}	−0.4525	0.8820	−0.0209	−0.0182	−0.0917	0.0898
v_{4j}	−0.0019	0.0046	−0.1718	−0.0905	0.7405	0.6433
v_{5j}	0.0372	−0.1279	−0.1938	−0.0678	−0.6652	0.7054
v_{6j}	0.8910	0.4533	−0.0067	−0.0037	−0.0172	0.0168
$\Delta x_{j,opt}$	−6.480	1.580	−2.376	3.856	−2.682	−0.153
$x_{j,opt}$	28.52	56.58	72.62	128.86	167.32	234.85

	$\langle B_{high}\rangle$	$\langle B_{low}\rangle$	F
x_{j0}	1.247	0.011	1.236
$x_{j,opt}$	1.266	0.014	1.251

between the core and the iron sectors, reducing $\langle B_{low}\rangle$, but the effect is small since B radial is already zero at the x axis due to the symmetry. On the other hand, the calculated flux density in the iron sectors is near the limit of the linear dependence of $B = \mu(Fe)H$ and the meniscus reduces its cross section, increasing B inside. In this region of the $B(H)$ curve of iron, a small increase of B would produce a large increase of H, expelling the flux lines, due to the continuity of the parallel components of H at the iron-air interface.

IV. EXPERIMENTAL MEASUREMENTS IN THE BUILT MAGNET

The built magnet (Fig. 3) was made with the initial FEM calculations, using single variations of the parameters and a further step looking to optimize the functional with each parameter. The effect of the nonzero susceptibility of the magnetocaloric material in the AMRs was also included. Moreover, the meniscus was finally not built, considering its small effect and the resulting easier construction without it. The final parameters were slightly different from the results of the full optimization described above. For our magnet, the radii were scaled to have a small system, but with

FIG. 3. Image of the magnet built with the specifications given in the text.

enough volume for the AMR to test different magnetocaloric materials with a good cooling power. The actual values of the construction were $\alpha_1 = 37^\circ$, $\alpha_2 = 56^\circ$, $\alpha_3 = 73^\circ$, $\beta_1 = 133^\circ$, $\beta_2 = 180^\circ$, $\beta_3 = 237^\circ$, $a = -e = 12.5$ mm, $b = 40$ mm, $c = 57$ mm, and $d = 100$ mm.

The length along the z direction was $L = 200$ mm. The main difference with the optimal values previously calculated is the increase of α_1, which saves the expensive material. This can be expressed in terms of Λ_{cool} [Eq. (1)], considering the important reduction of V_{mag}, against a small decrease of $\langle B_{high}^{2/3}\rangle - \langle B_{low}^{2/3}\rangle$. NdFeB for the sectors of permanent magnet was N48H, with a typical remanence $B_{rem} = \mu_0 M = 1.41$ T and intrinsic coercivity $\mu_0 H_c = 1.70$ T, preventing any risk of demagnetization for $B > -0.10$ T in the $\mathbf{M}$ direction. The iron sectors of the magnetic circuit were made with low-carbon nonalloy steel S235JR, having a permeability $\mu_r = 800$ at $B = 1.5$ T. The core was made of soft magnetic iron M600-50A, with $\mu_r = 1660$ at $B = 1.5$ T, in electrically insulated sheets perpendicular to the z axis to reduce eddy currents' dissipation. The magnetocaloric material filling the AMR increases the relative permeability of the gap from 1 to 2, which produces an important increase of the flux. For the given radii and lengths, the optimized values for the angles, $\alpha_1, \ldots, \beta_3$, considering the AMR space full of the magnetocaloric material with $\mu_r = 2$, resulted in a functional value $F = 1.251$. The built magnet keeps close to the optimized values the three most influential parameters, β_3, α_3, and α_2. The angle α_1 is markedly higher than the optimized value, but this deviation has a small influence on F,

reducing, on the other hand, the amount of permanent magnet used, and the also sizable deviations of β_1 and β_2 are even less important, as seen above. The resulting functional F, with the actual geometric parameters, decreases only to 1.234. Considering the dimensions of the magnet, the volume of the high field region restricted to its use in each AMR with $2\alpha = 45°$, and $\langle B^{2/3} \rangle$ calculated in the high and low field regions, the resulting figure of merit of Eq. (1) is $\Lambda_{cool} = 0.16$. Using the magnet with only four AMRs having $2\alpha = 90°$, gives $\Lambda_{cool} = 0.20$.

In Eq. (13), leaving out the very small reluctance of the iron parts of the circuit and defining the constant $\gamma = (l_{AMR}A_{mag})/(l_{mag}A_{AMR})$, the relative change of B_{AMR} with respect to an empty gap is $\Delta B/B = (\mu_r - 1)/(1 + \mu_r/\gamma)$, with μ_r being the relative permeability of the material filling the AMR. According to the geometrical data and the calculated field, the high flux in the gap covers a total angle of $2(90° - \alpha_3)$ (Fig. 2). Considering one half of the magnetic circuit, we can estimate $l_{mag} \simeq (c+d)(90-\alpha_1)\pi/180 = 145$ mm, $A_{mag} \simeq (d-c)L = 8600$ mm^2, $l_{AMR} \simeq 2(c-b) = 34$ mm, and $A_{AMR} \simeq (1/2)(b+c)L(90-\alpha_3)\pi/180 = 2878$ mm^2. With these values, it results $\gamma = 0.70$. Assuming $\mu_r \simeq 2$, an increase in the maximum field of about 26% can be expected when the AMR is completely filled with the magnetocaloric material, similar to the 21% increase given by the FEM calculations.

Measurements of the actual field were taken on the gap of the empty magnet using calibrated Hall probes for the longitudinal and transverse components, at different radial, angular and longitudinal positions, r, θ, 0 mm $\leq z \leq$ 200 mm, taking the center at $z = 100$ mm. Figure 4 shows these measured values at $z = 100$ mm, along the circle with the average radius of the AMRs region. The high and low field regions have values around $B_{\max} = 1.50$ T for $\theta = 0°$ and $B_{min} = 0.00$ T for $\theta = 90°$. Measurements taken in the gap, at 10 mm from the ends ($z = 10$ mm and 190 mm), showed a decrease of the radial component of 20% from the maximum field and a longitudinal component $B_z < 0.3$ T. The calculated values, using $\mu_r = 1$ to take into account that the measured region is empty of the magnetocaloric material, are also shown. A good agreement was found between the measured and calculated fields, using a value for the magnetization of the NdFeB sectors $\mu_0 M \simeq 1.33$ T, which is slightly lower than the reported typical value for the material used.

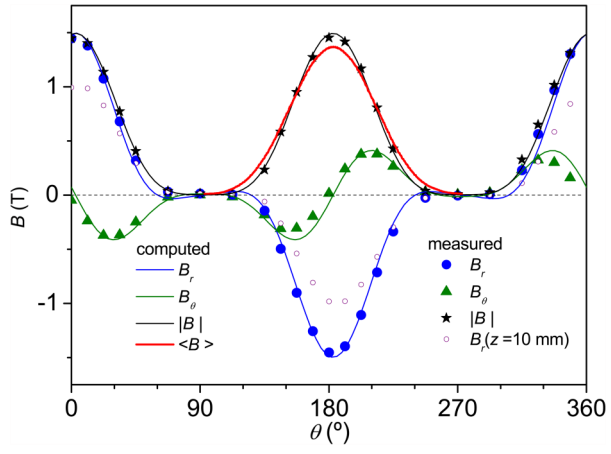

FIG. 4. Experimental measurements of the magnetic field in the radial and azimuthal directions, B_r and B_θ, at different points of the gap, compared with the calculated ones. A 183° shift has been applied to accommodate the computed values to the experiment. The magnetization value M is a scale factor in the calculations. The calculated and measured values agree for $\mu_0 M \simeq 1.33$ T. Hollow circles: Measured B_r at 10 mm from the end, show the field decay.

V. CONCLUSIONS

A simple method for optimizing the design of a magnetic circuit, intended for applications in magnetic refrigeration, has been developed. A finite element method has been used in the calculation of the magnetic field induction for each geometrical configuration of the magnet. The optimization procedure obtains the set of parameters x_i for the optimum functional $F(x_i)$ using a very limited number of evaluations of F, reducing the computation time. In this case, the functional F has been defined as the difference of the effective average magnetic field acting on a single regenerator in the region of high field, minus the same average in the region of low field. These averages have been calculated over each AMR that covers an angle of 45°. The optimized difference of average flux densities for this two-pole magnet with 12 hard magnetic sectors has been found to be $1.251\mu_0 M$. The magnetic field measured in an actual magnet built with optimized parameters agrees very well with the expected values from the calculations. The built magnet minimized the use of expensive hard magnets and gave a high volume for cooling material. The radial thickness of the gap for the AMRs allows an available volume for magnetocaloric material over 40% of the volume of NdFeB, and more than 50% of the magnet was completed with soft iron.

ACKNOWLEDGMENTS

The authors acknowledge the funding by the Spanish Ministerio de Ciencia, Innovación y Universidades (MICINN) and FEDER under Project Code No. MAT2017-86019-R.

REFERENCES

[1]V. K. Pecharsky and K. A. Gschneidner, Jr., Phys. Rev. Lett. **78**, 4494 (1997).
[2]A. Kitanoswki, J. Tusek, U. Tomc, U. Plaznik, M. Ozbolt, and A. Poredos, *Magnetocaloric Energy Conversion*, 1st ed. (Springer International Publishers, 2015), ISBN: 978-3-319-08740-5.
[3]R. Bjørk, C. R. H. Bahl, A. Smith, and N. Pryds, Int. J. Refrig. **33**, 437 (2010).
[4]X. Bohigas, F. Molins, A. Roig, J. Tejada, and X. Zhang, IEEE Trans. Magn. **36**, 538 (2000).
[5]R. Bjørk, C. R. H. Bahl, A. Smith, and N. Pryds, J. Magn. Magn. Mater. **322**, 3324 (2010).
[6]D. Eriksen, K. Engelbrecht, C. R. H. Bahl, R. Bjørk, K. K. Nielsen, A. R. Insinga, and N. Pryds, Int. J. Refrig. **58**, 14 (2015).
[7]A. Mira, T. de Larochelambert, C. Espanet, S. Giurgea, P. Nika, C. R. H. Bahl, R. Bøjrk, and K. K. Nielsen, J. Appl. Phys. **122**, 133901 (2017).
[8]C. Geuzaine and J. F. Remacle, Int. J. Numer. Methods Eng. **79**(11), 1309 (2009).
[9]P. Dular, C. Geuzaine, A. Genom, and W. Legros, IEEE Trans. Magn. **35**, 1682 (1999).
[10]W. H. Press, S. A. Teukolsky, W. T. Vetterling, and B. P. Flannery, *Numerical Recipes in Fortran77* (Cambridge University Press, 1997), ISBN: 0-521-43064-X.
[11]J. E. Dennis and J. J. Moree, Jr., SIAM Rev. **19**, 46 (1977).